Nanotechnology in the Life Sciences

Khalid Rehman Hakeem
Tanveer Bilal Pirzadah *Editors*

Nanobiotechnology in Agriculture

An Approach Towards Sustainability

Springer

Contents

Nanotechnology: A Boost for the Urgently Needed Second Green Revolution in Indian Agriculture

Kaizar Hossain, Syed Zaghum Abbas, Akil Ahmad, Mohd Rafatullah, Norli Ismail, Gaurav Pant, and Maruthi Avasn

1 Introduction

Agriculture is one of the major sectors that provide food for human, indirectly or directly in addition to feed, fibre, fire, and fuels. World agricultural industry is facing challenges such as climate change, urbanization, sustainable use of natural resources, and other environmental issues including urban runoff and accumulation of pesticides and fertilizers (Mukhopadhyay 2014). These problems are further intensified by an alarming population and food demand increment as an estimated population of 6–9 billion by 2050 is to be fed (Scott and Chen 2013; Chen and Yada 2011). India has targeted an average growth of 4% per annum for the agricultural sector by 2020 (Subramanian and Tarafdar 2011). However, India's agricultural growth has been experiencing decline during the last decade from about 3.6% (1985–1995) to less than 2% (1995–2005). Food grains production level is the major concern. The per capita annual production of cereals has shown declination from 200–205 kg in 1991/1995 to only 180–185 kg during 2004–2007, and it is still in decreasing trends which leads to great concerns towards food security. In order to achieve the 4% annual growth target, productivity and income per unit of these

K. Hossain (✉)
Department of Environmental Science, Asutosh College (Estd.- 1916), Kolkata, West Bengal, India

S. Z. Abbas · A. Ahmad · M. Rafatullah · N. Ismail
Environmental Technology Division, School of Industrial Technology, Universiti Sains Malaysia, Gelugor, Pulau Pinang, Malaysia

G. Pant
Institute of Applied Sciences and Humanities, GLA University, Mathura, Uttar Pradesh, India

M. Avasn
Department of Biosciences and Biotechnology, Krishna University, Machilipatnam, Andhra Pradesh, India

K. R. Hakeem, T. B. Pirzadah (eds.), *Nanobiotechnology in Agriculture*, Nanotechnology in the Life Sciences, https://doi.org/10.1007/978-3-030-39978-8_2

Environmental Science and Pollution Research
https://doi.org/10.1007/s11356-020-11061-y

SHORT RESEARCH AND DISCUSSION ARTICLE

Air quality assessment among populous sites of major metropolitan cities in India during COVID-19 pandemic confinement

Gaurav Pant[1] · Alka[2] · Deviram Garlapati[3] · Ashish Gaur[1] · Kaizar Hossain[4] · Shoor Vir Singh[1] · Ashish Kumar Gupta[5]

Received: 12 June 2020 / Accepted: 29 September 2020

Abstract

The present study aims to determine the impact of COVID-19 pandemic confinement on air quality among populous sites of four major metropolitan cities in India (Delhi, Mumbai, Kolkata, and Chennai) from January 1, 2020 to May 31, 2020 by analyzing particulate matter (PM2.5 and PM10), nitrogen dioxide (NO_2), ammonia (NH_3), sulfur dioxide (SO_2), carbon monoxide (CO), and ozone levels. The most prominent pollutant concerning air quality index (AQI) was determined by Pearson's correlation analysis and unpaired Welch's two-sample *t* test was carried out to measure the statistically significant reduction in average AQI for all the four sites. AQI significantly plummeted by 44%, 59%, 59%, and 6% in ITO-Delhi, Worli-Mumbai, Jadavpur-Kolkata, and Manali Village-Chennai respectively. The findings conclude a significant improvement in air quality with respect to reduction of 49–73%, 17–63%, 30–74%, and 15–58% in the mean concentration of PM2.5, PM10, NH_3, and SO_2 respectively during the confinement for the studied locations. The *p* values for all of the four studied locations were found significantly less than the 5% level of significance for Welch's *t* test analysis. In addition, reduced AQI values were highly correlated with prominent pollutants (PM2.5 and PM10) during Pearson's correlation analysis. These positive results due to pandemic imprisonment might aid to alter the current policies and strategies of pollution control for a safe and sustainable environment.

Keywords Air quality index · COVID-19 pandemic confinement · Pearson correlation analysis · Welch's *t* test analysis

Introduction

COVID-19 crisis is caused by coronavirus 2 (SARS-CoV-2), a severe acute respiratory syndrome (Jandrić 2020). Currently, India is undergoing a 4.0 phase of confinement and has 190,649 confirmed COVID-19 cases and 5406 deaths until May 31, 2020 (covid19india.org). Confinement in India or any part of the world ensures that all transportation, factories, construction work, restaurants, and other social places should be closed to follow the social distancing on a serious note. These confinement phases not only help to control the spreading of infection, but also offer improvement in planetary health.

Air pollution is a major subgroup of environmental pollution which poses a serious threat to the ecosystem. The risk of global sustainability can be reduced by controlling anthropogenic activities responsible for the emission of air pollutants in the environment. India accounts for having one of the most polluted capitals and cities within the globe (Guttikunda et al. 2019). During a study conducted by the Central Pollution Control Board (CPCB), the Ministry of Environment, India confirmed significant impact of 1-day confinement in the country (March 22, 2020), named as "Janata Curfew" of 14 h from 7 a.m. to 9 p.m., on air quality in terms of reducing pollutant level when compared with previous day data (Barkur and Vibha 2020) (source CPCB, India).

Keeping in view the above, in the present study, impact of COVID-19 confinement on air qualities among the populous site of four major metropolitan cities in India (i.e., site 1—

Responsible Editor: Marcus Schulz

✉ Gaurav Pant
rgauravpant@gmail.com; gaurav.pant@gla.ac.in

[1] Department of Biotechnology, Institute of Applied Sciences & Humanities, G.L.A. University, Mathura, Uttar Pradesh, India

[2] Department of Mathematics and Statistics, Banasthali Vidyapith, Banasthali, Rajasthan, India

[3] National Centre for Coastal Research, Ministry of Earth Sciences (MoES), Govt. of India, Chennai, India

[4] Department of Environmental Science, Asutosh College (Estd. - 1916), Kolkata, West Bengal, India

[5] Amity University, Noida, Uttar Pradesh, India

Published online: 11 October 2020

ITO, Delhi; site 2—Worli, Mumbai; site 3—Jadavpur, Kolkata; and site 4—Manali Village, Chennai) were determined by evaluating alteration in PM2.5, PM10, NO_2, NH_3, SO_2, CO, and ozone level from January 1, 2020 to May 31, 2020. Pearson product-moment correlation coefficient (PPMCC)-based model analysis was also proposed which determine the impact of COVID-19 pandemic confinement on air quality. Overall pandemic confinement has allowed the environment for detoxifying and renews itself in a lesser human interference phase. Environmental analysts designate it as a silver lining in terms of decreased carbon and waste emission but recognize it as a flawed perspective due to the expectation that the AQI levels to return as the coronavirus vanish and in some cases, they could come back strongly.

Origin of data set

Air quality index (AQI) reports daily air quality and its elevated level is associated with public health risks (Szyszkowicz 2019). Based on different national quality standards and dose-response relationships of pollutants, countries have different air quality indices (Zhang et al. 2020; Sofia et al. 2020). The Indian national air quality index considers eight pollutants (PM10, PM2.5, NO_2, SO_2, NH_3, CO, O_3, and Pb) with a 24-hourly averaging period. It is subdivided into six categories i.e., good (0–50), satisfactory (51–100), moderately polluted (101–200), poor (201–300), very poor (301–400), and severe (401–500) as shown in Fig. 1 (Perera 2018; Ghorani-Azam et al. 2016). The sub-indices for individual pollutants at a monitoring location are calculated using its 24-hourly average concentration value (8-hourly in case of CO and O_3) and health breakpoint concentration range. The worst sub-index is the AQI for that location (https://app.cpcbccr.com/AQI_India/). An increment in AQI causes acute and chronic mode health concern especially in the older age people and in children (Januszek et al. 2020; Pant et al. 2020). Due to the COVID-19 pandemic confinement, there is a significant reduction in the level of such toxic pollutants globally (Selvam et al. 2020; Singh and Chauhan 2020).

In the present study, concentrations of different pollutants i.e., PM2.5 (diameter < 2.5 μm), PM10 (diameter < 10 μm), NO_2, NH_3, SO_2, CO, ozone, and air quality index (AQI) were acquired from open access internet sources provided by the Central Pollution Control Board (CPCB), Ministry of Environment, Forests, and Climate Change (https://app.cpcbccr.com/AQI_India/). The data were recorded daily from January 1, 2020 to May 31, 2020, which is subdivided into two groups: (a) pre-lockdown period—January 1, 2020 to March 23, 2020, and (b) lockdown period—March 24, 2020 to May 31, 2020 at 17:00 IST among four different air quality monitoring stations of the CPCB for four major metropolitan cities in India i.e., site 1—ITO, Delhi, site 2—Worli, Mumbai, site 3—Jadavpur, Kolkata, and site 4—Manali Village, Chennai as shown in Fig. 2. For air quality assessment, % variations of air pollutants during the confinement period were compared with pre-lockdown values.

The air quality index is a piecewise linear function of the pollutant concentration. At the boundary between AQI categories, there is a discontinuous jump of one AQI unit. To convert from concentration to AQI, this equation is used:

$$I = \frac{I_{\text{high}} - I_{\text{low}}}{C_{\text{high}} - C_{\text{low}}} (C - C_{\text{low}}) + I_{\text{low}}$$

If multiple pollutants are measured, the calculated AQI is the highest value calculated from the above equation applied for each pollutant.where

I	The (air quality) index,
C	The pollutant concentration,
C_{low}	The concentration breakpoint that is $\leq C$,
C_{high}	The concentration breakpoint that is $\geq C$,
I_{low}	The index breakpoint corresponding to C_{low},
I_{high}	The index breakpoint corresponding to C_{high}.

Moreover, we have used unpaired Welch's two-sample t test analysis to measure the statistically significant reduction in average AQI for all four sites, as t test allows us to compare the average values of the two data sets and determine if they came from the same population. The formula for calculating t-statistics is given as:

$$t = \frac{\bar{x}_1 - \bar{x}_2}{\sqrt{\frac{s_1^2}{n_1} - \frac{s_2^2}{n_2}}}$$

where, $\bar{x}_1$ and $\bar{x}_2$ are the sample means, n_1 and n_2 are the sample sizes, and s_1^2 and s_2^2 are the sample variances for samples 1 and 2 respectively.

To find out the most prominent pollutant concerning AQI statistically, we have done Pearson's correlation analysis by the means of plotting heatmaps corresponding to each site. Pearson's correlation is also known as the "product-moment correlation coefficient" (PMCC) and is suitable for measuring the extent of the linear relationship between any two quantitative variables statistically. A Pearson's correlation is a number ranging between − 1 and + 1 showing negative to positive linear correlation. Given a pair of random variables (X_1, X_2),

Fig. 1 Indian national air quality index—category and range

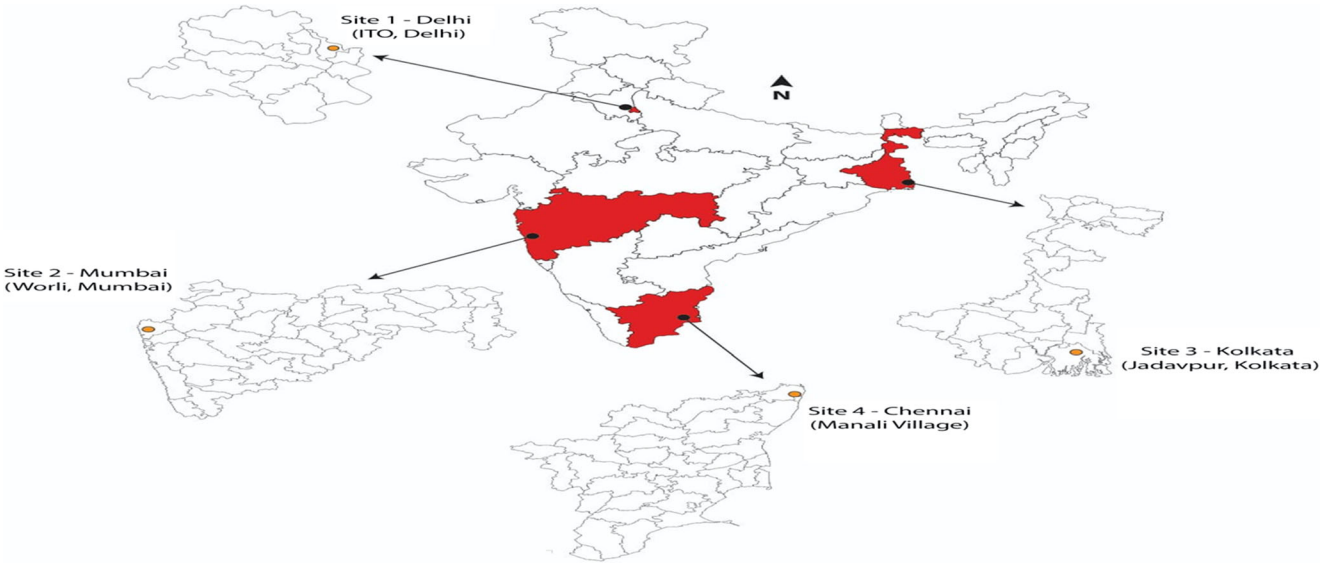

Fig. 2 The geography of monitoring stations among the populous sites of four major metropolitan cities in India

the formula for Pearson's correlation is given by

$$\rho_{X_1,X_2} = \frac{Cov(X_1,X_2)}{\sigma_{X_1}\,\sigma_{X_2}}$$

where $Cov(X_1,X_2)$ is the covariance between the variables under study and $\sigma_{X_1},\sigma_{X_2}$ are the standard deviation of X_1, X_2 respectively.

Analysis

Comparative study of AQI

In the present investigation, the AQI level was at its highest peak on year starting among all of the four studied sites i.e., 443 in site 1, 298 in site 2, 292 in site 3, and 166 in site 4. Initial data indicates Delhi was in the hazardous range while poor air quality in other states. Although irregular declining pattern was observed in the AQI level for all of the studied locations, a significant reduction within the pollutant level can be seen after comparing initial and final values. A remarkable drop falls of 44%, 59%, 59%, and 6% in mean concentration of AQI which was observed during COVID-19 pandemic confinement for sites 1, 2, 3, and 4 respectively as shown in Fig. 3.

Comparative study of air pollutants

Site 1—ITO, Delhi

Delhi, India's capital, is a massive metropolitan state in the northern area of the country and is among one of the most polluted capitals in the globe. Due to overpopulation and other responsible factors for urbanization, the pessimistic anthropogenic impact on the environment is at maximum. But, COVID-19 pandemic confinement facilitates the environment to retain its health which can be observed as a significant reduction in the air pollutant level in Delhi. At site 1—ITO, Delhi, during confinement period, the mean concentrations of PM2.5, PM10, NO_2, NH_3, and SO_2 significantly plummeted by 49%, 33%, 29%, 63%, and 24% respectively due to reduction in anthropogenic activities including traffic and manufacturing industries. Besides, due to high temperature and insolation during the confinement period, mean ozone concentration was highly elevated by 109% as shown in Table 1.

Site 2—Worli, Mumbai

Mumbai, the sixth most populous city in the world, is located on India's west coast and is the capital of Maharashtra. It is the financial, entertainment, and commercial center of India. During COVID-19 pandemic confinement, the second most populated city of India i.e., Mumbai has moved from poor to a satisfactory level of air quality. As initially at site 2, the values of the pollutants which were scattered around 200–300 μg/m^3 before confinement fallen to less than 60 μg/m^3 during the confinement period (Fig. 4). The mean concentration of PM2.5, PM10, NO_2, NH_3, SO_2, and CO, significantly reduced with a percentage of 73, 47, 86, 58, 58, 55, and 60 respectively due to shutdown of navigation activities and other industrial sectors with automobile transportation (Table 1). The drastic decline in nitrogen oxide levels over Mumbai is the result of reduced carbon-emission hotspots, industrial and coal combustion-dominated areas. A decrease in the concentration of urban ground-level ozone was recorded by 60% due to high reduction in nitrogen oxide concentration in the atmosphere.

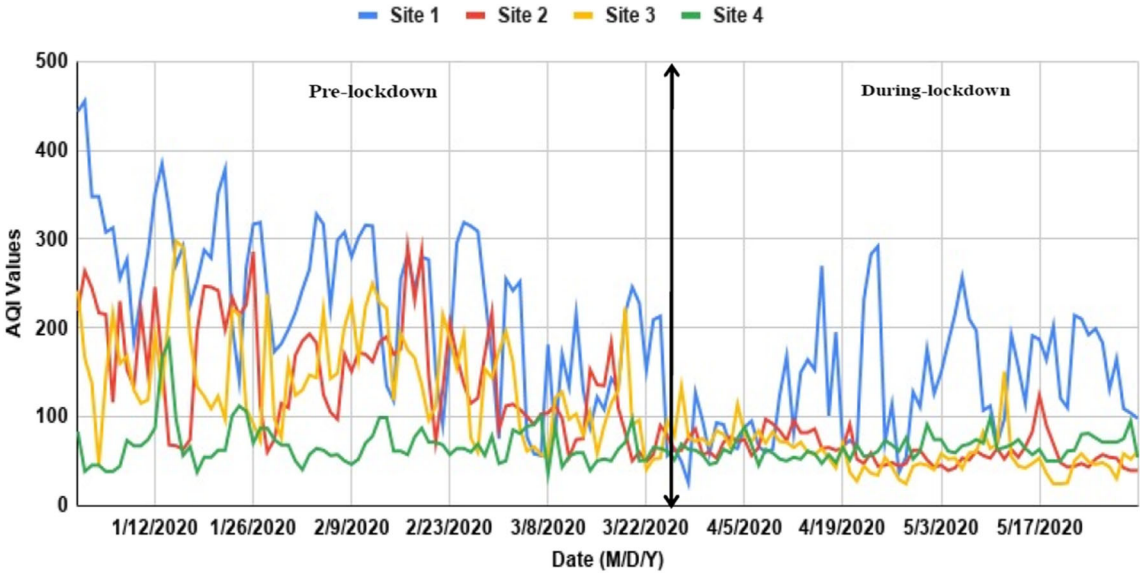

Fig. 3 Comparative AQI levels during pre-lockdown and lockdown period at 17:00 IST among four different air quality monitoring stations of the CPCB for four major metropolitan cities in India (site 1—ITO, Delhi, site 2—Worli, Mumbai, site 3—Jadavpur, Kolkata, and site 4—Manali Village, Chennai)

Site 3—Jadavpur, Kolkata

After Delhi and Mumbai, Kolkata is the third populous metropolitan area in the nation. Kolkata is the educational, cultural, and commercial center of the eastern part of the country and is the capital of West Bengal. The concentration of PM2.5, PM10, NO_2, NH_3, SO_2, and CO at site 3 significantly dropped steeply from 242, 205, 85, 10, 9, and 49 μg/m^3 as on January 1, 2020 to 20, 28, 9, 1, 7, and 22 μg/m^3 during COVID-19 pandemic confinement on May 31, 2020, respectively. Also, the mean concentration levels of PM2.5, PM10, NO2, NH3, SO2, and CO significantly reduced by 73%, 63%, 79%, 74%, 15%, and 32% due to decline in fossil fuel consumption, biomass burning, and other anthropogenic activities as observed from Fig. 4, while ozone levels were significantly raised by 77% with total variation of + 22 μg/m^3 during confinement period as similar to Delhi due to high winds, intermittent rains and thunderstorms, and high temperature and heatwaves.

Site 4—Manali Village, Chennai

Chennai, the capital of Indian state of Tamil Nadu, is the fourth urban agglomeration in the nation and is the 36th largest urban area by population in the world. It is located on the Coromandel Coast off the Bay of Bengal and is center for the

Table 1 Air quality assessment—variations and change (%) of average concentrations for different air pollutants during the pre and COVID-19 pandemic confinement, 2020 among populous sites of four major metropolitan cities in India

Pollutants	Pre-lockdown values				Lockdown				Variation and % change (pre-lockdown and lockdown)			
	Site 1	Site 2	Site 3	Site 4	Site 1	Site 2	Site 3	Site 4	Site 1	Site 2	Site 3	Site 4
AQI	238	151	144	68	134	62	59	64	− 104 (44%)	− 89 (59%)	− 86 (59%)	− 4 (6%)
PM2.5	238	132	135	56	122	36	36	26	− 116 (49%)	− 96 (73%)	− 99 (73%)	− 30 (54%)
PM10	150	116	122	60	100	61	45	49	− 50 (33%)	− 54 (47%)	− 77 (63%)	− 10 (17%)
NO_2	44	48	55	9	31	7	11	10	− 13 (29%)	− 41 (86%)	− 43 (79%)	1 (7%)
NH_3	10	2	8	14	4	1	2	9	− 6 (63%)	− 1 (58%)	− 6 (74%)	− 4 (30%)
SO_2	19	12	11	14	14	5	9	9	− 4 (24%)	− 7 (58%)	− 2 (15%)	− 6 (39%)
CO	53	28	33	25	84	13	22	35	31 (59%)	− 15 (55%)	− 11 (32%)	9 (37%)
O_3	35	85	29	36	73	34	51	65	38 (109%)	− 51 (60%)	22 (77%)	29 (80%)

PM2.5 in μg/m^3, PM10 in μg/m^3, CO in μg/m^3, NH_3 in μg/m^3, NO_2 in μg/m^3, SO_2 in μg/m^3, and O_3 in μg/m^3

AOI air quality index

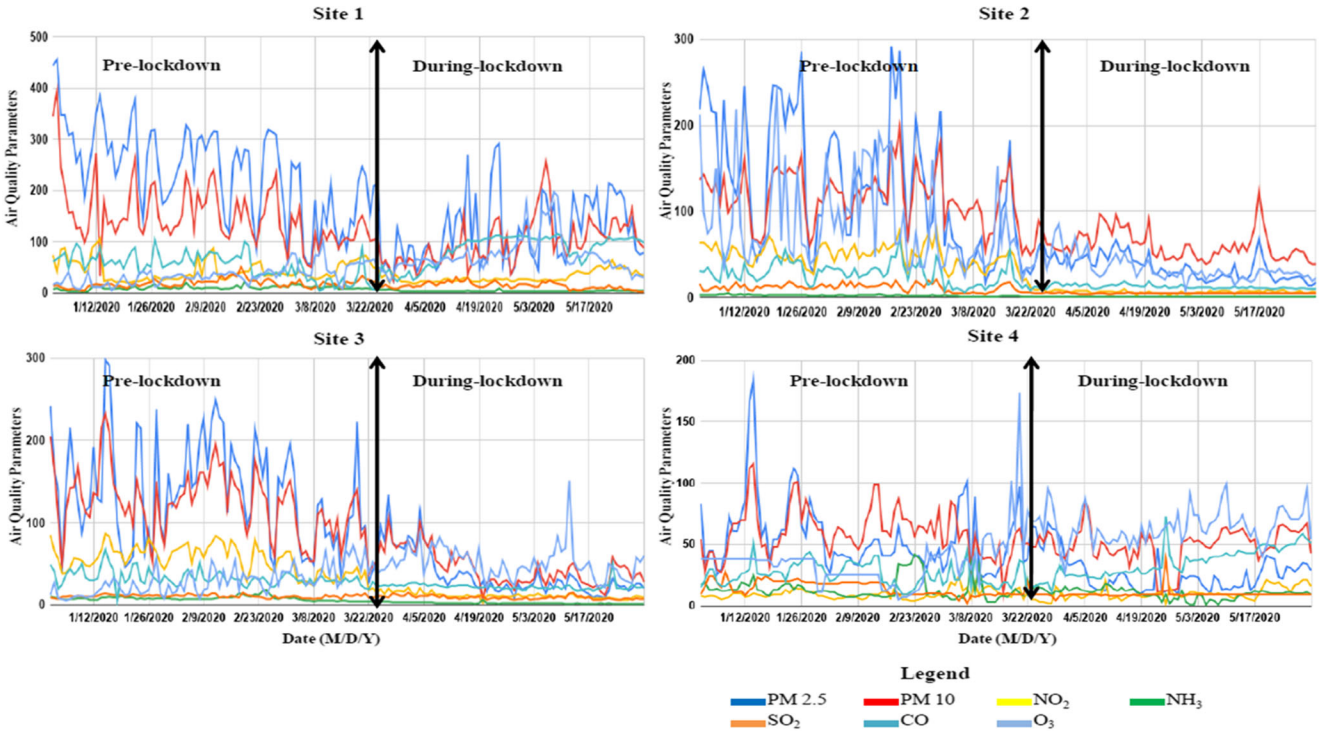

Fig. 4 The concentration of air pollutants (PM2.5 in μg/m^3, PM10 in μg/m^3, CO in μg/m^3, NH_3 in μg/m^3, NO_2 in μg/m^3, SO_2 in μg/m^3, and O_3 in μg/m^3) during pre-lockdown and lockdown period at 17:00 IST among four different air quality monitoring stations of the CPCB for four major metropolitan cities in India (site 1—ITO, Delhi, site 2—Worli, Mumbai, site 3—Jadavpur, Kolkata, and site 4—Manali Village, Chennai)

cultural, economical, and educational activities of south India. Similar to all other studied sites, the air quality of site 4—Manali Village, Chennai also confirmed improvement in terms of reduction in pollutant level during the confinement period. The mean concentrations of PM2.5, PM10, NH_3, and SO_2 were reduced by 54%, 17%, 30%, and 39% respectively as shown in Fig. 4, while due to fuel and coal burning, vehicular emissions, and continuous functioning of power plants in the neighborhood of site 4, there was no significant reduction in NO_2 (+ 1 μg/m^3), CO (+ 9 μg/m^3), and ozone levels (+ 29 μg/m^3) (https://www.cag.org.in/blogs/air-quality-chennai-during-lockdown-do-we-have-clues-mitigate-air-pollution).

Pearson correlation analysis

The Pearson correlation coefficient was determined by constructing a heatmap for the concentration of various pollutants (pre and during pandemic confinement) among populous sites of four metropolitan cities of India, viz. ITO, Delhi, Worli, Mumbai, Jadavpur, Kolkata, and Manali Village, Chennai.

Site 1—ITO, Delhi

At this site, the perfect positive correlation was observed between AQI and PM2.5, a strong positive correlation between AQI-PM10 and PM2.5-PM10, whereas a negative correlation was observed for ozone with AQI and other pollutants. The correlation coefficient between AQI-PM2.5, AQI-PM10, and PM2.5-PM10 was found as 0.98, 0.82, and 0.77 respectively, showing a significantly higher positive relationship. This indicate the changes in PM2.5 and PM10 concentrations have a great influence on AQI content; i.e., an increase in their concentration will directly elevate the air quality index. Besides, AQI-ozone, PM2.5-ozone, and PM10-ozone confirmed low negatively correlated variables, i.e., − 0.31, − 0.38, and − 0.18 respectively indicating the higher values of AQI, PM2.5, and PM10 will lower down the ozone concentration. A feeble correlation exists between AQI-NH_3 (0.46), AQI-NO_2 (0.38), AQI-SO_2 (0.28), and AQI-CO (0.11) showing mild effect on AQI (Fig. 5 (a)).

Site 2—Worli, Mumbai

Product-moment correlation coefficient analysis for site 2 demonstrates the positive correlation between all of the studied pollutants as shown in Fig. 5 (b). The highest correlations were confirmed between AQI-PM2.5, with a correlation of 0.97, AQI-PM10, with 0.94, and PM2.5-PM10, with 0.91 which demonstrates PM2.5 and PM10 are the most significant dominating factors in elevating the AQI. A correlation value of 0.80, 0.74, 0.72, and 0.86 between AQI-NO_2, AQI-NH_3, AQI-SO_2, and AQI-CO indicates a significant positive relationship, while moderate correlation was determined between CO and ozone concentration (0.53).

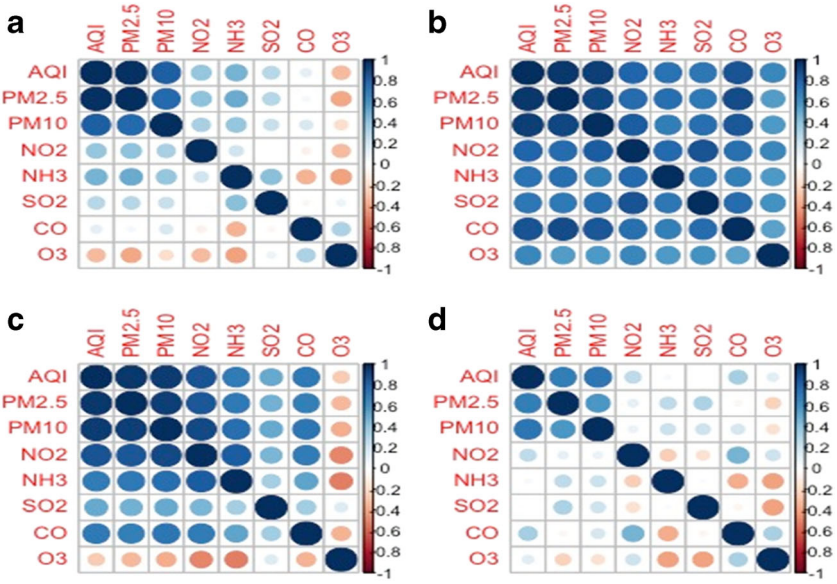

Fig. 5 Pearson's correlation heatmap for air pollutants during the pre and COVID-19 pandemic confinement, 2020 among populous sites of four major metropolitan cities in India

Site 3—Jadavpur, Kolkata

A significant positive correlation was observed between the prominent pollutants PM2.5, PM10, NO_2, NH_3, and CO with AQI, i.e., 0.96, 0.95, 0.86, 0.70, and 0.70 respectively in site 3 as shown in Fig. 5 (c). This implies the studied pollutants had a great impact on air quality among monitoring station of Jadavpur, Kolkata, whereas ozone shows a negative correlation with AQI (− 0.25), and other studied pollutants i.e., PM2.5 (− 0.32), PM10 (− 0.36), NO_2 (− 0.48), NH_3 (− 0.50), and CO (− 0.35). This indicates mean O_3 concentration will significantly increase with a decrease in the mean AQI, PM2.5, PM10, NO_2, NH_3, and CO concentrations.

Site 4—Manali Village, Chennai

Pearson's correlation heatmap for Manali Village, Chennai demonstrates significant positive correlations for PM2.5 (0.69) and PM10 (0.73) with AQI, while other pollutants exhibit a moderate or negative correlation. The lowest values of correlation coefficient were found for the pairs AQI-NO_2 (0.26), AQI-NH_3 (0.04), and AQI-CO (0.33) indicating mild association between these variables; i.e., the effect of concentration of NO_2, NH_3, and CO on air quality is minimal. However, the approximately zero correlation between AQI-SO_2 (0.009) and AQI-ozone (0.01) indicates no linear relationship, but there may be some other strong non-linear relationship between the two variables (Fig. 5 (d)). In other words, we can say that the simple linear function cannot describe its relationship in depth.

Inferential t-statistic (Welch's two-sample *t* test)

In the present study, the significant impact of COVID-19 pandemic confinement on air quality in studied locations was determined by right-tailed, Welch's two-sample *t* test. The complete data set was divided into two groups, pre-confinement (A) and during confinement (B) to assess if there is a statistically significant effect of confinement on AQI. Independent random samples of sizes n_1, n_2 were drawn by using a random number table from both the groups and applied *t* test using the R-software. This inferential statistic was used to test the following hypothesis:

> H_0: No significant difference between the means of two groups i.e., no significant effect of COVID-19 pandemic confinement on AQI ($\mu_1 = \mu_2$).
> H_A: Significant difference between the means of two groups i.e., air quality is significantly improved during COVID-19 pandemic confinement ($\mu_1 > \mu_2$), where μ_1 and μ_2 are the population means of the two groups.

From Table 2, we can observe that the t-statistic (5.91), which when compared with critical *t* value (1.67) at 5% level of significance (α), rejected the null hypothesis and confirmed the significant reduction in the AQI for site 1. The *p* value was also found to be very small, suggesting that the COVID-19 pandemic confinement reduced AQI (45%). The *p* value revealed it is "unlikely" that we would observe such an extreme test statistic *t** in the direction of H_A if the null hypothesis was true. Therefore, the initial assumption that the null hypothesis is true must be incorrect. That is, since the *p* value, 0.00000015, is very less than $\alpha = 0.05$, we reject the null

Table 2 Welch's two-sample *t* test analysis

	Site 1		Site 2		Site 3		Site 4	
	Sample A	Sample B	Sample A	Sample B	Sample A	Sample B	Sample A	Sample B
Mean	241.65	134.25	159.12	65.77	144.86	57.45	75.78	63.20
Observations	36	35	36	35	36	35	36	35
Hypothesized mean difference	0		0		0		0	
Degree of freedom	62		38		40		42	
95% confidence interval	(71.05, 143.75)		(69.45, 116.99)		(63.14, 111.65)		(1.09, 24.05)	
t-statistic	5.91		7.94		7.28		2.20	
P ($T \leq t$) one-tail	0.00000015		0.0000000014		0.0000000074		0.03	
t Critical one-tail	1.67		1.68		1.68		1.68	

hypothesis $H_0 : \mu_1 = \mu_2$ in favor of the alternative hypothesis $H_A : \mu_1 > \mu_2$. However, if we lowered our willingness to make a type I error to $\alpha = 0.01$ instead, the significant rejection of the null hypothesis is again observed. This is due to reduction in anthropogenic activities including fuel and coal burning, vehicular emissions, and manufacturing industries.

The same behavior can be observed from the data of Table 2 for 2nd, 3rd, and 4th studied locations where the much lowered *p* values exhibited the statistically significant effect of COVID-19 pandemic confinement in lowering the sample mean AQI by 58%, 60%, and 17% respectively.

Conclusion

The present study demonstrates the impact of COVID-19 pandemic confinement on air quality among the populous site of four major metropolitan cities in India i.e., site 1—ITO, Delhi, site 2—Worli, Mumbai, site 3—Jadavpur, Kolkata, and site 4—Manali Village, Chennai. A data set was constructed for AQI, PM2.5, PM10, NO_2, NH_3, SO_2, CO, and ozone from January 1, 2020 to May 31, 2020 from the Central Pollution Control Board (CPCB). Pearson's correlation analysis and Welch's *t* test were performed for the determination of statistically significant improvement in the air quality during the confinement period. A remarkable drop falls of 44%, 59%, 59%, and 6% in AQI which was observed during COVID-19 pandemic confinement in sites 1, 2, 3, and 4 respectively. It can be concluded that remarkable improvement in the air quality during confinement period was observed as the *p* values of the test for all of the four sites were very less than the significance level ($\alpha = 0.05$). Besides, the Welch's *t* test was supported by findings of Pearson's correlation analysis in which the prominent pollutants (PM2.5 and PM10) were also found to be highly correlated with AQI. Although a significant impact on planetary health can be noticed during COVID-19 pandemic confinement, the circumstance is momentary and limits for a short duration i.e., only up to confinement period.

Acknowledgments The authors are grateful to the Central Pollution Control Board (CPCB), Ministry of Environment, Forests, and Climate Change, India for providing open access to internet sources which help in the construction of data set for the current study. The authors would like to convey their sincere thanks to the management of G.L.A. University, Mathura (U.P.), India, Department of Mathematics and Statistics, Banasthali Vidyapith, Banasthali, Rajasthan, India, National Centre for Coastal Research, Ministry of Earth Science (MoES), Govt. of India, Chennai, India, Department of Environmental Science, Asutosh College (Estd. - 1916), Kolkata, West Bengal, India, and Amity University, Noida, Uttar Pradesh, India for providing facilities.

Authors' contribution All authors have a specific role in the current research and have contributed to the preparation of the article. Preparation of the data set was performed by Dr. Gaurav Pant, Dr. Alka, and Dr. Deviram Garlapati. The validation and effectiveness of the proposed models were studied by Dr. Gaurav Pant, Dr. Alka, Dr. Kaizar Hossain, and Mr. Ashish Gaur, while Dr. Gaurav Pant, Dr. Alka, Dr. SV Singh, and Dr. AK Gupta were actively involved in article structure and analysis.

Data availability The data sets analyzed during the current study are available in the open access internet sources provided by the Central Pollution Control Board (CPCB), Ministry of Environment, Forests, and Climate Change (https://app.cpcbccr.com/AQI_India/).

Compliance with ethical standards

Conflict of interest The authors declare that they have no conflict of interest.

Consent to participate Not applicable.

Consent to publish Not applicable.

References

Barkur G, Vibha GBK (2020) Sentiment analysis of nationwide lockdown due to COVID 19 outbreak: evidence from India. Asian J Psychiatr 12:102089. https://doi.org/10.1016/j.ajp.2020.102089

Ghorani-Azam A, Riahi-Zanjani B, Balali-Mood M (2016) Effects of air pollution on human health and practical measures for prevention in Iran. J Res Med Sci: the official journal of Isfahan University of Medical Sciences 21:65. https://doi.org/10.4103/1735-1995.189646

Guttikunda SK, Nishadh KA, Jawahar P (2019) Air pollution knowledge assessments (APnA) for 20 Indian cities. Urban Clim 27:124–141. https://doi.org/10.1016/j.uclim.2018.11.005

Jandrić P (2020) Postdigital research in the time of Covid-19. Postdigit Sci Educ 2:233–238. https://doi.org/10.1007/s42438-020-00113-8

Januszek R, Staszczak B, Siudak Z, Bartuś J, Plens K, Bartuś S, Dudek D (2020) The relationship between increased air pollution expressed as PM10 concentration and the frequency of percutaneous coronary interventions in patients with acute coronary syndromes—a seasonal differences. Environ Sci Pollut Res 27:21320–21330. https://doi.org/10.1007/s11356-020-08339-6

Pant G, Yadav DP, Gaur A (2020) ResNeXt convolution neural network topology-based deep learning model for identification and classification of Pediastrum. Algal Res 48:101932. https://doi.org/10.1016/j.algal.2020.101932

Perera F (2018) Pollution from fossil-fuel combustion is the leading environmental threat to global pediatric health and equity: solutions exist. Int J Environ Res Public Health 15(1):16. https://doi.org/10.3390/ijerph15010016

Selvam S, Muthukumar P, Venkatramanan S, Roy PD, Bharath KM, Jesuraja K (2020) SARS-CoV-2 pandemic lockdown: effects on air quality in the industrialized Gujarat state of India. Sci Total Environ 737:140391. https://doi.org/10.1016/j.scitotenv.2020.140391

Singh RP, Chauhan A (2020) Impact of lockdown on air quality in India during COVID-19 pandemic. Air Qual Atmos Health 13:921–928. https://doi.org/10.1007/s11869-020-00863-1

Sofia D, Gioiella F, Lotrecchiano N, Giuliano A (2020) Mitigation strategies for reducing air pollution. Environ Sci Pollut Res 27:19226–19235. https://doi.org/10.1007/s11356-020-08647-x

Szyszkowicz M (2019) The Air Quality Health Index and all emergency department visits. Environ Sci Pollut Res 26:24357–24361. https://doi.org/10.1007/s11356-019-05741-7

Zhang N, Zhao K, Yu Y (2020) The effect of environmental regulation on air pollution, productivity, and factor structure: a quasi-natural experiment evidence from China. Environ Sci Pollut Res 27:20392–20409. https://doi.org/10.1007/s11356-020-08462-4

Algal Research 50 (2020) 102018

Contents lists available at ScienceDirect

Algal Research

journal homepage: www.elsevier.com/locate/algal

Short communication

Deep learning-based ResNeXt model in phycological studies for future

D.P. Yadav[a], A.S. Jalal[a], Deviram Garlapati[b], Kaizar Hossain[c], Ayush Goyal[d], Gaurav Pant[e,*]

[a] Department of Computer Engineering & Applications, G.L.A. University, Mathura, U.P., India
[b] National Centre for Coastal Research, Ministry of Earth Science (MoES), Govt. of India, Chennai, India
[c] Department of Environmental Science, Asutosh College (Estd. - 1916), Kolkata, West Bengal, India
[d] Department of Biotechnology, G.L.A. University, Mathura, U.P., India
[e] Department of Electrical Engineering and Computer Science, Texas A & M University Kingsville, Kingsville, TX, USA

ARTICLE INFO

Keywords:
Data augmentation
Algal genera
Convolution neural network
ResNeXt topology

ABSTRACT

Algae are photosynthetic eukaryotes that may range from unicellular to multicellular forms. Algae have been reported from almost all the ecological systems, including terrestrial, marine, and aquatic ecosystems. The manual classification of algae is a time-consuming method and requires great efforts with expertise due to the numerous families and genera. In the present study, an automated system is developed for the identification and classification of the 16 algal families with a data set of 80,000 images by a modified ResNeXt CNN (Convolution Neural Network) model. Cell differentiation by modified ResNeXt CNN topology is based on cell arrangement and morphological features including area, width, shape, and length of the cell. An experimental result of 99.97% classification accuracy demonstrates the effectiveness of the proposed method. The present investigation may open a new path in the future for the development of a time and a cost-effective, highly sensitive computer-based system for the identification and classification of different algae.

1. Introduction

Water is a fundamental component of life [1]. But due to various natural and anthropogenic activities, quality and quantity of water bodies are reducing globally [2,3]. Harmful algal blooms (HABs) are one of the major agents, affecting water quality due to their ability for producing various toxins [4,5]. Algae are photosynthetic eukaryotes that may range from unicellular to multicellular forms and produce a wide range of bioactive substances in which some are classes of toxins [6,7]. Various environmental conditions such as high concentrations of nutrients, particularly phosphorus, high water temperature, long hydraulic retention time, stable water body stratification, etc., favor algal bloom formation [8,9]. Regulatory and specialized agencies concerned with public health have introduced specific water quality protocols concerning algae for potable water. These risk management approaches are based on hazard assessment by algal identification, determination, and limitation of critical control points [10,11]. Therefore types and threshold levels of algal species have become critical for ensuring successful water management. As the manual identification of algae requires expertise and great efforts, a computer-based automated system with high accuracy may open a new path for the development of time and a cost-effective approach [12]. The advanced machine learning technique like deep learning is an emerging and effective tool for the identification and differentiation of different algal genera. Similar to manual identification, automated technique classifies algal cells based on the morphological characters and parameters including area, width, shape, and length of the cell [13].

For the last few decades some studies reported, different automated models such as a convolutional neural network (CNN), neural architecture search (NAS), artificial neural networks (ANN), etc. for algal identification. Promdaen et al. [14] demonstrate an automated recognition system with computing texture descriptors, feature combination approach, and Sequential Minimal Optimization (SMO) for the identification of 12 microalgae found in water resources of Thailand. They confirmed the effectiveness of the method in terms of 97.22% classification accuracy. Li et al. [15] demonstrate a promising and efficient solution via the Mueller matrix imaging system based on convolutional neural networks (CNNs) for the automatic classification of morphologically similar algae. They worked on a data set contains 10,463 Mueller matrices and achieve 97% classification accuracy. Deglint et al. [16] developed an innovative system with 96% accuracy for classifying six algal genera using a pre-trained deep residual convolution neural network. Park et al. [13] developed an effective CNN model for the classification of eight algal genera from watersheds with an F1-score of 0.95. They conclude the automated system as an emerging tool with high efficiency and rapid responses for monitoring algal events in

* Corresponding author at: Department of Biotechnology, Institute of Applied Sciences & Humanities, G.L.A. University, Mathura, U.P., India.
E-mail address: gaurav.pant@gla.ac.in (G. Pant).

https://doi.org/10.1016/j.algal.2020.102018
Received 28 May 2020; Received in revised form 14 July 2020; Accepted 18 July 2020
Available online 27 July 2020

water bodies. Santaquiteria et al. [17] demonstrate a differential segmentation approach for diatoms by an automated system for grading water quality. With the dataset of 126 images of 10 different taxa, debris and fragments they improved a sensitive system with an average sensitivity of 95%, the specificity of 60%, and precision to 57%. Besides, they also demonstrate an instance segmentation approach that was able to separate the overlapping of diatoms.

Although some studies in the past have been reported, which solve automated identification problem for algae, however, most of the previous studies classify few algal families with less range of morphologically similar groups with the pre-trained model. There is ample scope to develop such automatic techniques with high learning ability for the quandary. More recently, to perform an automated identification and classification task for seven *Pediastrum* species within a data set of 42,000 images, we proposed an efficient modified ResNeXt CNN model [18]. The proposed modified model was developed by reducing parameters including kernel size and filter size from the original ResNeXt CNN model. Classification accuracy, ROC curve area, and F1-score of 98.45%, 99%, and 0.98 respectively, demonstrate the high effectiveness of the proposed method. In view to our previous work, an attempt has been made in the present study for the identification and classification of the 16 algal families including *Peranemataceae*, *Phormidiaceae*, *Nostocaceae*, *Ceratiaceae*, *Chlamydomonadaceae*, *Euglenaceae*, *Scenedesmaceae*, *Dunaliellaceae*, *Volvocaceae*, *Cyanophoraceae*, *Gymnodiniaceae*, *Oocystaceae*, *Oocystaceae*, *Oscillatoriaceae*, *Peridiniaceae* and *Euglenaceae* by modified ResNeXt CNN model. In the future, such algorithms will support various phycological and water management studies as a cost and time effective facilities.

2. Material and methods

2.1. Proposed method

In the present study, algae classification is performed a using modified ResNeXt CNN model derived from the residual network as mentioned by Pant et al. [18]. The proposed model contains ReLu activation, residual blocks, grouped convolution, and the final dense layer was used in softmax optimizer. The architecture of the proposed ResNeXt CNN model is shown in Fig. 1. In a deep learning model grouped convolutions allow to build a wide network by replicating the filters in a module. This process reduces the computation by obtaining feature maps from kernel filters [19]. The Leaky ReLu activation function was used to remove gradient decent problems and to avoid saturation of the model [20].

In the proposed model Leaky ReLu activation is used after batch normalization. The inner product can be a consideration as a form of aggregating transformation

$$\sum_{i=1}^{N} w_i y_i \tag{1}$$

where, $y = (y_1, y_2, y_3 \ldots\ldots y_N)$ i.e. N channel input vector to the neuron. The filter weight of the i^{th} neurons is given by w_i.

Elementary transformation ($w_i y_i$) was replaced with a more generic function, which itself can also be a network. Aggregated transformations can be presented as:

$$\mathrm{T}(y) = \sum_{i=1}^{C} V_i(y) \tag{2}$$

where, $V_i(y)$ is an arbitrary function. Analogous to a simple neuron, V_i should project y into an (optionally low dimensional) embedding and then transform it. The residual block of the proposed model can be defined as:

$$x = y + \sum_{i=1}^{C} V_i(y) \tag{3}$$

where, $x =$ the output of the proposed model, $C =$ the cardinality of the model and, $y =$ input vectors to neurons. The final dense layer contains a softmax optimizer which converts logits into the probability of change to a particular algal class. This probability value can be calculated based on input weight and bias. Finally, the value is converted to the class value of the algae. Eqs. (4) and (5) are used to calculate the value for softmax optimizer.

$$\mathrm{P}(y = i \mid \Phi^{(j)}) = \frac{e^{\Phi^{(j)}}}{\sum_{i=0}^{N} e^{\Phi_N^{(J)}}} \tag{4}$$

$$\Phi = w_0 x_0 + w_1 x_1 + \ldots\ldots\ldots\ldots + w_N x_N \tag{5}$$

where, $\Phi =$ input vector, $w_0 x_0 =$ the bias of the i^{th} class, $N =$ 16 (algal genera classes). The value of $i =$ 0 to 15, the index and corresponding class representation can be given as:

i = {0: *Anabaena*, 1: *Arthrospira*, 2: *Anisonema*, 3: *Ceratium*, 4: *Chlamydomonas*, 5: *Cyclidiopsis*, 6: *Desmodesmus*, 7: *Dunaliella*, 8: *Eudorina*, 9: *Glaucophyta*, 10: *Gymnodinium*, 11: *Kirchneriella*, 12: *Oonephris*, 13: *Oscillaroria*, 14: *Peridinium*, 15: *Phyacus*}. The network was trained with the image size 256 × 256 × 3 and cardinality hyperparameter C = 32. The final dense layer is adjusted to 16 class

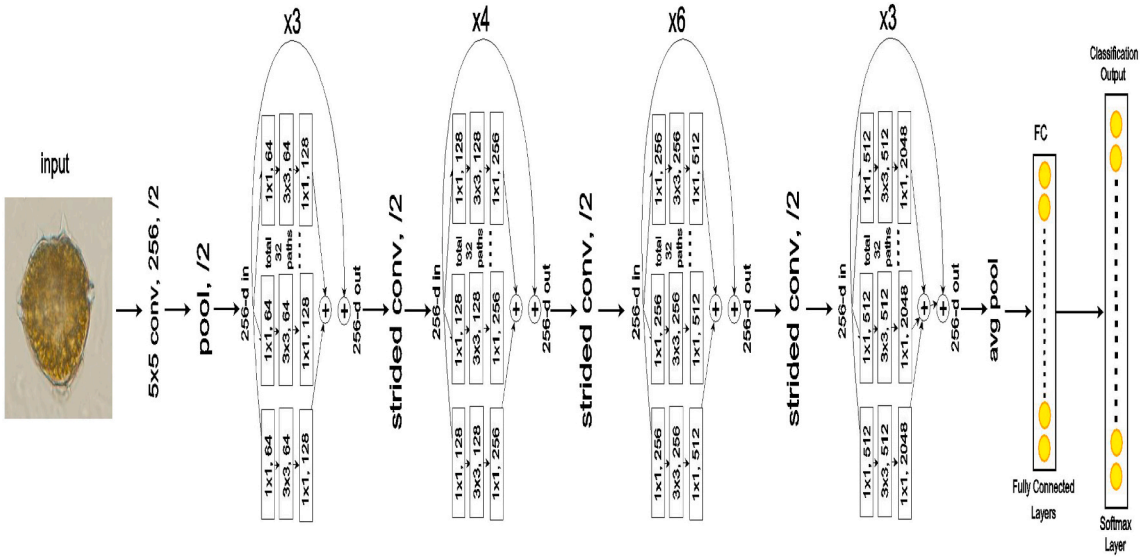

Fig. 1. The modified ResNeXt model architecture for the classification of the 16 algal genera.

classification. The network is trained to 20 epochs and took a computing time of approximately 14 h on an Nvidia GeForce GTX TITAN X GPU.

3. Results and discussion

3.1. Dataset

In the present study, the dataset was constructed for 16 algal families. Algal images were collected from different open access internet sources and previous phycological studies carried out by authors, similarly as mentioned by Pant et al. [18]. The original dataset contains 100 algal images.

3.2. Data augmentation

The size of the dataset was enhanced up to 80,000 images by using techniques described by Pant et al. [18]. The augmented dataset was constructed in such a way so that an equal number of images were distributed in each class. For training and validation of the model, 80% (64,000) and 20% (16,000) of images are randomly fractionated.

3.3. Training and validation

Based on the morphological characteristics, algal genera were categorized as unicellular and multicellular forms as shown in Fig. 2. Before training and validation, the input size was attuned to adopt the image of size 256 × 256 pixels. The initial learning rate was set to $1e^{-3}$ with a batch size of 15. The labeling of each class was performed in both the training and the validation images. The network was compiled with the Adam optimizer.

The performance of the system was evaluated by the parameters accuracy (ACC), precision (Pre), recall (Re), and F1-score from the confusion matrix which can be defined as:

$$ACC = \frac{Tp + Tn}{Tp + Tn + Fp + Fn} \quad (6)$$

$$\mathrm{Pre} = \frac{Tp}{Tp + Fp} \quad (7)$$

$$\mathrm{Re} = \frac{Tp}{Tp + Fn} \quad (8)$$

$$F1 - score = 2 * \frac{\mathrm{Pre} * \mathrm{Re}}{\mathrm{Pre} + \mathrm{Re}} \quad (9)$$

where, *Tp* (true-positive), *Fp* (false- positive), *Fn* (false-negative) and *Tn* (true-negative).

The training loss (Trn-Loss) and the testing loss (Ts_Loss) were calculated by the categorical_crossentropy. The training and the testing accuracy and Trn-Loss and the Ts_Loss are shown in Fig. 3. The training and testing accuracy of the proposed network was 100 and 99.97%, while training and testing loss were found as 0.04 and 0.06% respectively. Results indicate the outstanding performance of the model for classifying algal genera in the present study. Although, loss in training and testing can be further reduced by running the model for more epochs. The important factor to decide the number of epochs is based on the validation error of the proposed model. For example, if the validation error starts increasing that might be an indication of overfitting. In such a case the model should be set on the number of epochs as high as possible and terminate training based on the error rates. After running the model for several epochs, the model accuracy starts saturating. The minimum number of epochs that saturates the accuracy should be fixed for the proposed model. In the present study, the model gets saturated after 20 epochs. We also conducted another experiment by running the system on 25 epochs. In which, the validation loss decreases to 0.002., but there was no change in the training and classification accuracy. Thus, the minimum number of epochs was set at 20.

3.4. The error matrix

In the present study, an error matrix was plotted for the sensitivity determination of the proposed model as described by Pant et al. [18]. The rows and columns represent predicted classes and their instances respectively. Similar morphological features between different algal species may influence the sensitivity of automated models. Various studies have been reported for the reduction in accuracy during automated classification due to the same features and cellular arrangements of algal classes. Giraldo-Zuluaga et al. [21] reported a reduction in classification accuracy of the Artificial Neural Network (ANN) model by misclassification of *Scenedesmus* sp. due to similar cell shape and texture. A similar observation was reported by Pant et al. [18] during the automated classification of seven *Pediastrum* species by modified ResNeXt CNN topology in which 30 false positive and negative values were obtained during the error matrix analysis in a dataset of 42,000 images. The misclassification of algal species with similar morphological characteristics can be reduced through the training of a model with less noised image and large training dataset. A very high deep learning model for example 150 layers deep learning model can also be used to reduce misclassification [22]. The classification accuracy achieved by the proposed model was optimal and acceptable. In the

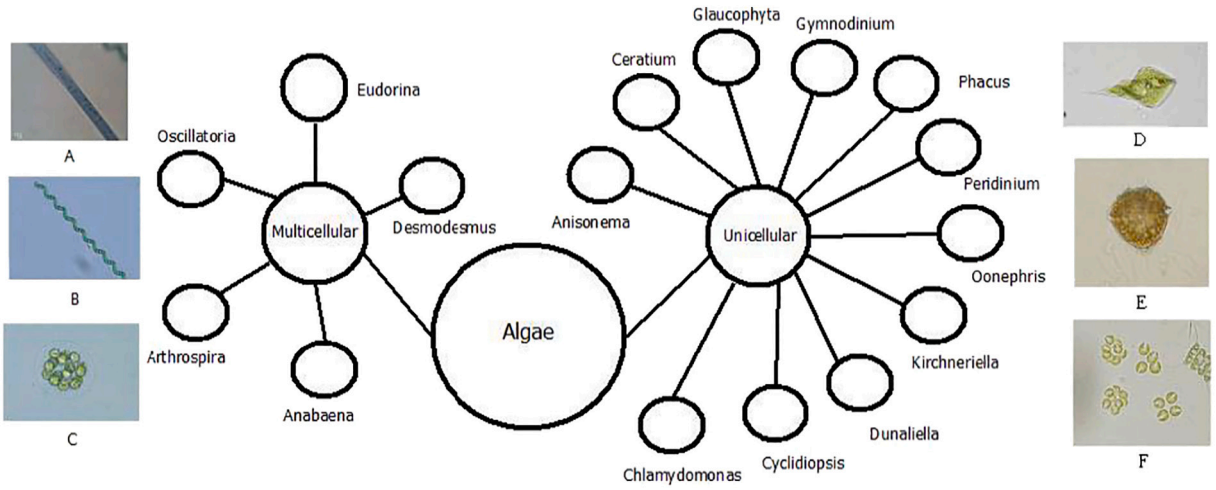

Fig. 2. Classification of 16 algal genera based on the morphological features.

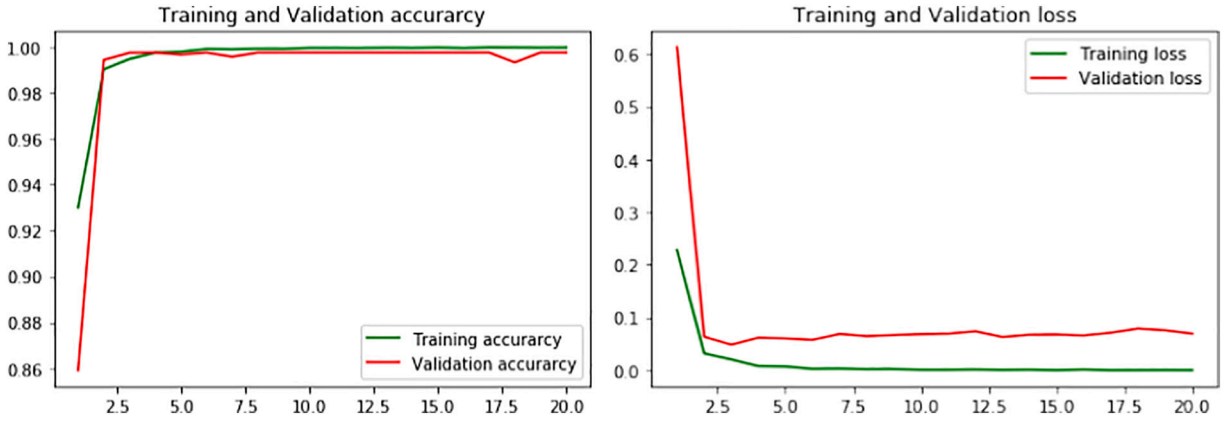

Fig. 3. Training and validation of the proposed model with accuracy and loss.

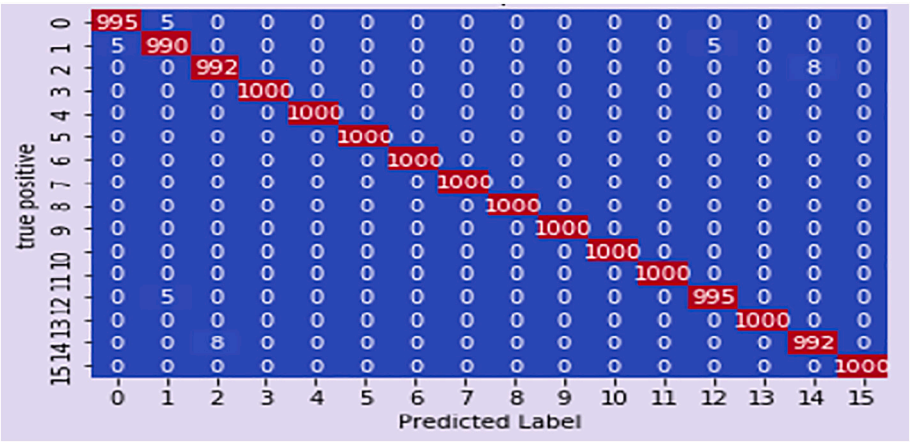

Fig. 4. Confusion matrix of the proposed model.

present study, confusion matrix for the *Anabaena* and *Arthrospira*, false-positive value, and false-negative value is 5 within the testing dataset i.e. 5 images of *Anabaena* are wrongly predicted to Arthrospira, due to the similarities including filamentous morphological shape and presence of helical trichomes. While due to similarties as coiled morphology and unflagellated ovoid green unicells, five images of the genus *Arthrospira* and *Oonephris* are misclassified with each other. Besides, similarities like biflagellate flattened ovoid shape and armoured dinoflagellates in *Anisonema* with *Peridinium* are affinity causing factors as shown in Fig. 4.

3.5. F1-score and Receiver Operating Characteristic (ROC) curve

The performance of the model was measured by the precision, recall, and F1-score. The class-wise performance measured of the algal genera [23]. In the previous study Pant et al. [18], seven classes of *Pediastrum* were identified and classified by the modified ResNeXt CNN model. But due to very high morphological similarities among algal species, an increase in false-positive value with a decrease in true positive values were observed, which reduces precision. While in the present study due to less morphological similarities between 16 algal families the false-positive values were less and true positive values were high. Thus the precision of the proposed model increased up to 0.99. Among 16 algal species studied, the F1 score reaches its best value at 1 (i.e. perfect precision and recall) for 11 classes i.e. for *Ceratium*, *Chlamydomonas*, *Cyclidiopsis*, *Desmodesmus*, *Dunaliella*, *Eudorina*, *Glaucophyta*, *Gymnodinium*, *Kirchneriella*, *Oscillatoria*, and *Phyacus*, while for *Anabaena*, *Arthrospira*, *Anisonema*, *Oonephris*, and *Peridinium*, F1 score demonstrates very high prediction values (Table 1).

Table 1
The class-wise performance measure (F1-score) of the proposed model.

S. no.	Algae	Precision	Recall	F1 - score
0	*Anabaena*	0.99	0.99	0.99
1	*Arthrospira*	0.99	0.99	0.99
2	*Anisonema*	0.99	0.99	0.99
3	*Ceratium*	1	1	1
4	*Chlamydomonas*	1	1	1
5	*Cyclidiopsis*	1	1	1
6	*Desmodesmus*	1	1	1
7	*Dunaliella*	1	1	1
8	*Eudorina*	1	1	1
9	*Glaucophyta*	1	1	1
10	*Gymnodinium*	1	1	1
11	*Kirchneriella*	1	1	1
12	*Oonephris*	0.99	0.99	0.99
13	*Oscillatoria*	1	1	1
14	*Peridinium*	0.99	0.99	0.99
15	*Phyacus*	1	1	1

Receiver Operating Characteristic (ROC) analysis is also performed for accuracy evaluation of the proposed automated model. The ROC curves for 16 class algal classification were more than 99% as shown in Fig. 5. The ROC curves of some classes are very closed to 100%. The effectiveness of the proposed modified deep ResNeXt CNN topology measured using different parameters is notable.

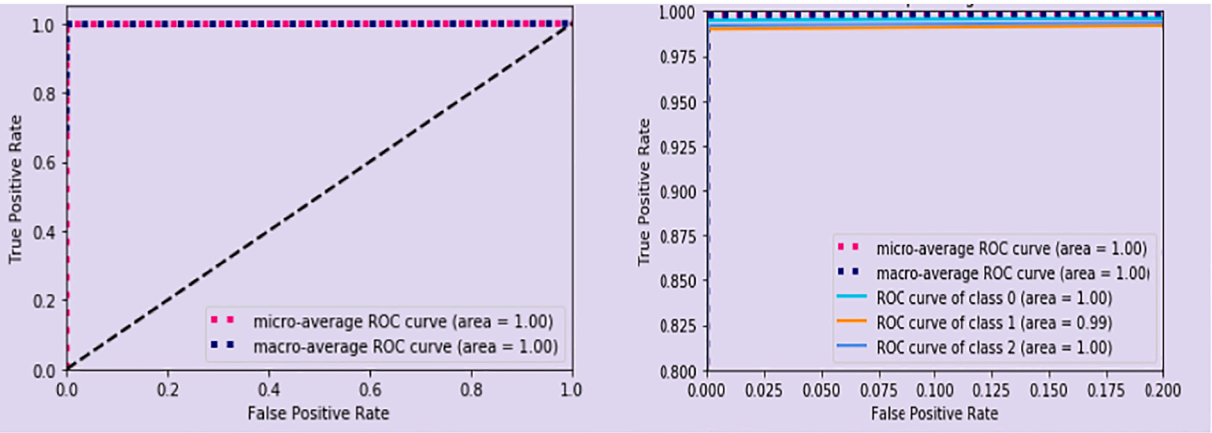

Fig. 5. The ROC curve of the proposed model and class-wise ROC curve area.

4. Conclusion

In the present study, a deep learning-based algorithm has been developed to reduce time and dependency on an expert for algal identification by modified ResNeXt CNN topology. The proposed model confirms high accuracy and acceptable loss during training and validation for an augmented data set consisting of 80,000 images of 16 algal species. In addition to very little affinity in confusion matrix and 99% ROC curve area, the effectiveness of the proposed model is determined by high F1-score, training accuracy, and classification accuracy i.e. 99.9%, 100%, and 99.97% respectively. This accuracy is much better than the state-of-the-art methods. In the future study, we will add more algae class for the classification. The proposed models also need to test on the other dataset, so that the performance of the system can be further evaluated.

Funding

This research did not receive any specific grant from funding agencies in the public, commercial, or not-for-profit sectors.

Ethical statement

This article does not contain any studies with human participants or animals performed by any of the authors.

CRediT authorship contribution statement

D.P. Yadav: Conceptualization, Data curation, Methodology, Validation.**A.S. Jalal**:Supervision, Visualization.**Deviram Garlapati**:Investigation.**Kaizar Hossain**:Investigation.**Ayush Goyal**: Data curation, Formal analysis.**Gaurav Pant**:Project administration, Writing - original draft, Writing - review & editing.

Declaration of competing interest

All of the authors declare that he has no conflict of interest. We certify that the submission is original work and neither the submitted materials nor portions have been published previously or are under consideration for publication elsewhere.

Acknowledgment

The authors are grateful to GLA University, Mathura, U.P. for support in the present research. Authors would like to convey their sincere thanks to the Department of Biotechnology, IAH, GLA University, Mathura, India; Department of Computer Engineering & Applications, G.L.A. University, Mathura, India; National Centre for Coastal Research, Ministry of Earth Science (MoES), Govt. of India, Chennai, India; Department of Environmental Science, Asutosh College (Estd. - 1916), Kolkata, West Bengal, India and Department of Electrical Engineering and Computer Science, Texas A & M University Kingsville, Kingsville, TX, USA. for providing facilities for research.

References

[1] M. Singh, G. Pant, K. Hossain, A.K. Bhatia, Green remediation. Tool for safe and sustainable environment: a review, Appl Water Sci 7 (2017) 2629–2635.
[2] Li-Hua Li, Xin-Yu Li, Yu Hong, Meng-Ran Jiang, Lu Song-Liu, Use of microalgae for the treatment of black and odorous water: purification effects and optimization of treatment conditions, Algal Res. 47 (2020) 101851, https://doi.org/10.1016/j.algal.2020.101851.
[3] G. Pant, A. Singh, M. Panchpuri, R.G. Prasuna, K. Hossain, S.Z. Abbas, A. Ahmad, N. Ismail, M. Rafatullah, Enhancement of biosorption capacity of cyanobacterial strain to remediate heavy metals, Desalin. Water Treat. 165 (2019) 244–252.
[4] L. Shang, Z. Hu, Y. Tang, Identification of dissolved and particulate carbonyl compounds produced by marine harmful algal bloom species, J. Ocean. Limnol. 37 (2019) 1566–1581.
[5] Di Pan, Shruti Pavagadhi, Shivshankar Umashankar, Amit Rai, Peter I. Benke, Megha Rai, Gourvendu Saxena, Vamshidhar Gangu, Sanjay Swarup, Resource partitioning strategies during toxin production in Microcystis aeruginosa revealed by integrative omics analysis, Algal Res. 42 (2019) 101582.
[6] M.L. Wells, P. Potin, J.S. Craigie, Algae as nutritional and functional food sources: revisiting our understanding, J. Appl. Phycol. 29 (2017) 949–982.
[7] Ana L. Pereira, Catarina Santos, Joana Azevedo, Teresa P. Martins, Raquel Castelo-Branco, Vitor Ramos, Vitor Vasconcelos, Alexandre Campos, Effects of two toxic cyanobacterial crude extracts containing microcystin-LR and cylindrospermopsin on the growth and photosynthetic capacity of the microalga Parachlorella kessleri, Algal Res. 34 (2018) 198–208.
[8] J.S. Kim, I.W. Seo, D. Baek, Seasonally varying effects of environmental factors on phytoplankton abundance in the regulated rivers, Sci. Rep. 9 (1) (2019) 9266–9278.
[9] Jinling Cai, Minglang Chen, Guangce Wang, Guanghua Pan, Peng Yu, Fermentative hydrogen and polyhydroxybutyrate production from pretreated cyanobacterial blooms, Algal Res. 12 (2015) 295–299.
[10] R. Altenburger, W. Brack, R.M. Burgess, et al., Future water quality monitoring: improving the balance between exposure and toxicity assessments of real-world pollutant mixtures, Environ. Sci. Eur. 31 (2019) 12–29.
[11] Jonathan Gressel, Cécile J.B. van der Vlugt, Hans E.N. Bergmans, Environmental risks of large scale cultivation of microalgae: mitigation of spills, Algal Res. 2 (3) (2013) 286–298.
[12] N. Santhi, C. Pradeepa, P. Subashini, S. Kalaiselvi, Automatic identification of algal community from microscopic images, Bioinforma. Biol. Insights 7 (2013) 327–334.
[13] J. Park, H. Lee, C.Y. Park, S. Hasan, T.Y. Heo, W.H. Lee, Algal morphological identification in watersheds for drinking water supply using neural architecture search for convolutional neural network, Water 11 (2019) 1338–1357.
[14] S. Promdaen, P. Wattuya, N. Sanevas, Automated microalgae image classification, Procedia Comput. Sci. 29 (2014) 1981–1992.
[15] Xianpeng Li, Ran Liao, Jialing Zhou, Priscilla T.Y. Leung, Meng Yan, Hui Ma, Classification of morphologically similar algae and cyanobacteria using Mueller matrix imaging and convolutional neural networks, Appl. Opt. 56 (2017) 6520–6530.
[16] J.L. Deglint, C. Jin, A. Wong, Investigating the automatic classification of algae using the spectral and morphological characteristics via deep residual learning, in: F. Karray, A. Campilho, A. Yu (Eds.), Image Analysis and Recognition. ICIAR 2019. Lecture Notes in Computer Science, vol 11663, Springer, Cham, 2019.
[17] J.R. Santaquiteria, G. Bueno, O. Deniz, N. Vallez, G. Cristobal, Semantic versus

instance segmentation in microscopic algae detection, Eng. Appl. Artif. Intell. 87 (2020) 103271–103286.
[18] G. Pant, D.P. Yadav, A. Gaur, ResNeXt convolution neural network topology-based deep learning model for identification and classification of Pediastrum, Algal Res. 48 (2020) 101932, , https://doi.org/10.1016/j.algal.2020.101932.
[19] G. Zhao, Z. Zhang, H. Guan, P. Tang, J. Wang, Rethinking ReLU to train better CNNs, 2018 24th International Conference on Pattern Recognition (ICPR), IEEE, 2018, pp. 603–608. August.
[20] R. Zhao, W. Luk, Learning Grouped Convolution for Efficient Domain Adaptation, arXiv preprint, 2018. arXiv:1811.09341.
[21] J.H. Giraldo-Zuluaga, A. Salazar, G. Diez, A. Gomez, T. Martínez, J.F. Vargas, M. Peñuela, Automatic identification of Scenedesmus polymorphic microalgae from microscopic images, Pattern. Anal. Applic. 21 (2) (2018) 601–612.
[22] T.J. Durant, E.M. Olson, W.L. Schulz, R. Torres, Very deep convolutional neural networks for morphologic classification of erythrocytes, Clin. Chem. 63 (12) (2017) 1847–1855.
[23] A. Tharwat, Classification assessment methods, Appl. Comput. Inform. (2018), https://doi.org/10.1016/j.aci.2018.08.003 In Press.